



Study of $\psi(2S)$ production and cold nuclear matter effects in $p\text{Pb}$ collisions at $\sqrt{s_{NN}} = 5 \text{ TeV}$

The LHCb collaboration[†]

Abstract

The production of $\psi(2S)$ mesons is studied in dimuon final states using proton-lead collision data collected by the LHCb detector. The data sample corresponds to an integrated luminosity of 1.6 nb^{-1} . The nucleon-nucleon centre-of-mass energy of the proton-lead collisions is $\sqrt{s_{NN}} = 5 \text{ TeV}$. The measurement is performed using $\psi(2S)$ mesons with transverse momentum less than $14 \text{ GeV}/c$ and rapidity y in the ranges $1.5 < y < 4.0$ and $-5.0 < y < -2.5$ in the nucleon-nucleon centre-of-mass system. The forward-backward production ratio and the nuclear modification factor are determined for $\psi(2S)$ mesons. Using the production cross-section results of $\psi(2S)$ and J/ψ mesons from b -hadron decays, the $b\bar{b}$ cross-section in $p\text{Pb}$ collisions at $\sqrt{s_{NN}} = 5 \text{ TeV}$ is obtained.

Submitted to JHEP

© CERN on behalf of the LHCb collaboration, licence CC-BY-4.0.

[†]Authors are listed at the end of this paper.

1 Introduction

The quark-gluon plasma (QGP) is a state of matter with asymptotically free partons, which is expected to exist at extremely high temperature and density. It is predicted that heavy quarkonium production will be significantly suppressed in ultrarelativistic heavy-ion collisions if a QGP is created [1]. This suppression is regarded as one of the most important signatures for the formation of the QGP. Heavy quarkonium production can also be suppressed in proton-nucleus (pA) collisions, where hot nuclear matter, *i.e.* QGP, is not expected to be created and only cold nuclear matter (CNM) effects exist. Such CNM effects include: initial-state nuclear effects on the parton densities (shadowing); coherent energy loss consisting of initial-state parton energy loss and final-state energy loss; and final-state absorption by nucleons, which is expected to be negligible at LHC energies [2–9]. The study of pA collisions is important to disentangle the effects of QGP from those of CNM, and to provide essential input to the understanding of nucleus-nucleus collisions.

Nuclear effects are usually characterized by the nuclear modification factor, defined as the production cross-section of a given particle per nucleon in pA collisions divided by that in proton-proton (pp) collisions,

$$R_{pA}(y, p_T, \sqrt{s_{NN}}) \equiv \frac{1}{A} \frac{d^2\sigma_{pA}(y, p_T, \sqrt{s_{NN}})/dydp_T}{d^2\sigma_{pp}(y, p_T, \sqrt{s_{NN}})/dydp_T}, \quad (1)$$

where A is the atomic mass number of the nucleus, y (p_T) is the rapidity (transverse momentum) of the produced particle, and $\sqrt{s_{NN}}$ is the centre-of-mass energy of the proton-nucleon system. Throughout this paper, y always indicates the rapidity in the nucleon-nucleon centre-of-mass system.

The suppression of quarkonium and light hadrons at large rapidity has been observed in pA collisions [10–13] and in deuteron-gold collisions [14–18]. The proton-lead (pPb) collisions recorded at the LHC in 2013 enable the study of CNM effects at the TeV scale. With these pPb data, the production cross-sections of prompt J/ψ mesons, J/ψ mesons from b -hadron decays, and Υ mesons were measured, and the CNM effects were studied by determining the nuclear modification factor R_{pPb} and the forward-backward production ratio R_{FB} [19, 20]. Working in the nucleon-nucleon rest frame, the “forward” and “backward” directions are defined with respect to the direction of the proton beam. The ratio R_{FB} is defined as

$$R_{FB}(y, p_T, \sqrt{s_{NN}}) \equiv \frac{\sigma_{pPb}(+|y|, p_T, \sqrt{s_{NN}})}{\sigma_{pPb}(-|y|, p_T, \sqrt{s_{NN}})}. \quad (2)$$

The advantage of measuring this ratio is that it does not rely on knowledge of the production cross-section in pp collisions. Furthermore, part of the experimental systematic uncertainties and theoretical scale uncertainties cancel in the ratio.

Previous measurements in fixed-target pA collisions by E866 [10], NA50 [11] and HERA-B [12] showed that the production cross-sections for both J/ψ and $\psi(2S)$ mesons

are suppressed in pA collisions compared with those in pp collisions. These measurements also showed stronger suppression at central rapidity for $\psi(2S)$ mesons than for J/ψ mesons, while at forward rapidity the suppressions were compatible within large uncertainties. The PHENIX experiment made similar observations in dAu collisions at RHIC [18]. The ALICE experiment measured the $\psi(2S)$ suppression in pPb collisions at the LHC [21]. Nuclear shadowing and energy loss predict equal suppression of J/ψ and $\psi(2S)$ mesons, and so cannot explain the observations. One explanation is that the charmonium states produced at central rapidity spend more time in the medium than those at forward rapidities; therefore the loosely bound $\psi(2S)$ mesons are more easily suppressed than J/ψ mesons at central rapidity [22–24]. In this picture it is expected that the charmonium states will spend a much shorter time in the CNM at LHC energies than at lower energies, leading to similar suppression for $\psi(2S)$ and J/ψ mesons even at central rapidity.

The excellent reconstruction resolution of the LHCb detector for primary and secondary vertices [25] provides the ability to separate prompt $\psi(2S)$ mesons, which are produced directly from pp collisions, from those originating from b -hadron decays (called “ $\psi(2S)$ from b ” in the following). In this analysis, the production cross-sections of prompt $\psi(2S)$ mesons and $\psi(2S)$ from b are measured in pPb collisions at $\sqrt{s_{NN}} = 5$ TeV. The nuclear modification factor R_{pPb} and the forward-backward production ratio R_{FB} are determined in the range $2.5 < |y| < 4.0$. Using the production cross-sections of $\psi(2S)$ from b and J/ψ from b , the $b\bar{b}$ production cross-section in pPb collisions is obtained.

2 Detector and datasets

The LHCb detector [25,26] is a single-arm forward spectrometer covering the pseudorapidity range $2 < \eta < 5$, designed for the study of particles containing b or c quarks. The detector includes a high-precision tracking system consisting of a silicon-strip vertex detector surrounding the pPb interaction region, a large-area silicon-strip detector located upstream of a dipole magnet with a bending power of about 4 Tm, and three stations of silicon-strip detectors and straw drift tubes placed downstream of the magnet. The tracking system provides a measurement of momentum, p , of charged particles with a relative uncertainty that varies from 0.5% at low momentum to 1.0% at 200 GeV/ c . The minimum distance of a track to a primary vertex, the impact parameter, is measured with a resolution of $(15 + 29/p_T)$ μm , where p_T is the component of the momentum transverse to the beam, in GeV/ c . Different types of charged hadrons are distinguished using information from two ring-imaging Cherenkov detectors. Photons, electrons and hadrons are identified by a calorimeter system consisting of scintillating-pad and preshower detectors, an electromagnetic calorimeter and a hadronic calorimeter. Muons are identified by a system composed of alternating layers of iron and multiwire proportional chambers. The online event selection is performed by a trigger, which consists of a hardware stage, based on information from the calorimeter and muon systems, followed by a software stage, which applies a full event reconstruction.

With the proton beam travelling in the direction from the vertex detector to the muon

system and the lead beam circulating in the opposite direction, the LHCb spectrometer covers forward rapidities. With reversed beam directions backward rapidities are accessible. The data sample used in this analysis is collected from the $p\text{Pb}$ collisions in early 2013, corresponding to an integrated luminosity of 1.1 nb^{-1} (0.5 nb^{-1}) for forward (backward) collisions. The instantaneous luminosity was around $5 \times 10^{27} \text{ cm}^{-2} \text{ s}^{-1}$, five orders of magnitude below the nominal LHCb luminosity for pp collisions. Therefore, the data were taken using a hardware trigger which simply rejected empty events. The software trigger for this analysis required one well-reconstructed track with hits in the muon system and p_{T} greater than $600 \text{ MeV}/c$.

Simulated samples based on pp collisions at 8 TeV are used to determine the acceptance and reconstruction efficiencies. The simulation samples are reweighted so that the track multiplicity distribution reproduces the experimental data of $p\text{Pb}$ collisions at 5 TeV. In the simulation, pp collisions are generated using PYTHIA [27] with a specific LHCb configuration [28]. Decays of hadronic particles are described by EVTGEN [29], in which final-state radiation is generated using PHOTOS [30]. The interaction of the generated particles with the detector, and its response, are implemented using the GEANT4 toolkit [31] as described in Ref. [32].

3 Event selection and cross-section determination

The measurement of $\psi(2S)$ production is based on the method described in Refs. [19,33,34]. The $\psi(2S)$ candidates are reconstructed using dimuon final states from events with at least one primary vertex. The tracks should be of good quality, have opposite sign charges and be identified as muons with high p_{T} . The two muon tracks are required to originate from a common vertex with good vertex fit quality, and the reconstructed $\psi(2S)$ mass should be in the range $\pm 145 \text{ MeV}/c^2$ around the known $\psi(2S)$ mass [35].

Due to the small size of the data sample, only one-dimensional differential cross-sections are measured. The differential production cross-section of $\psi(2S)$ mesons in a given kinematic bin is defined as

$$\frac{d\sigma}{dX} = \frac{N}{\mathcal{L} \times \mathcal{B} \times \Delta X}, \quad (3)$$

where X denotes p_{T} or y , N is the efficiency-corrected number of $\psi(2S)$ signal candidates reconstructed with the dimuon final state in the given bin of X , ΔX is the bin width, \mathcal{L} is the integrated luminosity, and \mathcal{B} is the branching fraction of the $\psi(2S) \rightarrow \mu^+\mu^-$ decay, $\mathcal{B}(\psi(2S) \rightarrow \mu^+\mu^-) = (7.9 \pm 0.9) \times 10^{-3}$ [35]. Assuming lepton universality in electromagnetic decays, this branching fraction is replaced by that of the $\psi(2S) \rightarrow e^+e^-$, which has a much smaller uncertainty, $\mathcal{B}(\psi(2S) \rightarrow e^+e^-) = (7.89 \pm 0.17) \times 10^{-3}$ [35].

The integrated luminosity of the data sample used in this analysis was determined using a van der Meer scan, and calibrated separately for the $p\text{Pb}$ forward and backward samples [36]. The kinematic region of the measurement is $p_{\text{T}} < 14 \text{ GeV}/c$ and $1.5 < y < 4.0$ ($-5.0 < y < -2.5$) for the forward (backward) sample. For the single differential cross-section measurements, the transverse momentum range $p_{\text{T}} < 14 \text{ GeV}/c$ is divided into five

bins with edges at (0, 2, 3, 5, 7, 14) GeV/ c . The rapidity range is divided into five bins of width $\Delta y = 0.5$.

4 Signal extraction and efficiencies

The numbers of prompt $\psi(2S)$ and $\psi(2S)$ from b in each kinematic bin are determined from an extended unbinned maximum likelihood fit performed simultaneously to the distributions of the dimuon invariant mass $M_{\mu\mu}$ and the pseudo proper decay time t_z [33], defined as

$$t_z = \frac{(z_\psi - z_{\text{PV}}) \times M_\psi}{p_z}, \quad (4)$$

where z_ψ is the position of the $\psi(2S)$ decay vertex along the beam axis, z_{PV} that of the primary vertex refitted after removing the two muon tracks from the $\psi(2S)$ candidate, p_z the z component of the measured $\psi(2S)$ momentum, and M_ψ the known $\psi(2S)$ mass [35].

The invariant mass distribution of the signal in each bin is modelled by a Crystal Ball (CB) function [37], where the tail parameters are fixed to the values found in simulation and the other parameters are allowed to vary. For differential cross-section measurements, the sample size in each bin is very small. Therefore, in order to stabilise the fit, the mass resolution of the CB function is fixed to the value obtained from the J/ψ sample, scaled by the ratio of the $\psi(2S)$ mass to the J/ψ mass. The invariant mass distribution of the combinatorial background is described by an exponential function with variable slope parameter. The signal distribution of t_z can be described [38] by a δ -function at $t_z = 0$ for prompt $\psi(2S)$ and an exponential function for the component of $\psi(2S)$ from b , both convolved with a Gaussian resolution function. The width of the resolution function and the slope of the exponential function are free in the fit. The background distribution of t_z in each kinematic bin is modelled with an empirical function determined from sidebands of the invariant mass distribution.

Figure 1 shows projections of the fit to $M_{\mu\mu}$ and t_z for the full $p\text{Pb}$ forward and backward samples. The combinatorial background in the backward region is higher than that in the forward region, because the track multiplicity in the backward region is larger. The mass resolution is 13 MeV/ c^2 for both the forward and backward samples. The total estimated signal yield for prompt $\psi(2S)$ mesons in the forward (backward) sample is 285 ± 34 (81 ± 23), and that for $\psi(2S)$ from b in the forward (backward) sample is 108 ± 16 (21 ± 8), where the uncertainties are statistical only.

The efficiency-corrected signal yield N is obtained from the sum of w_i/ε_i over all candidates in the given bin. The weight w_i is obtained with the *sPlot* technique using $M_{\mu\mu}$ and t_z as discriminating variables [39]. The total efficiency ε_i , which depends on p_{T} and y , includes the geometrical acceptance, the reconstruction efficiency, the muon identification efficiency, and the trigger efficiency. The acceptance and reconstruction efficiencies are determined from simulation, assuming that the produced $\psi(2S)$ mesons are unpolarised. The efficiency of the muon identification and the trigger efficiency are obtained from data using a tag-and-probe method as described below.

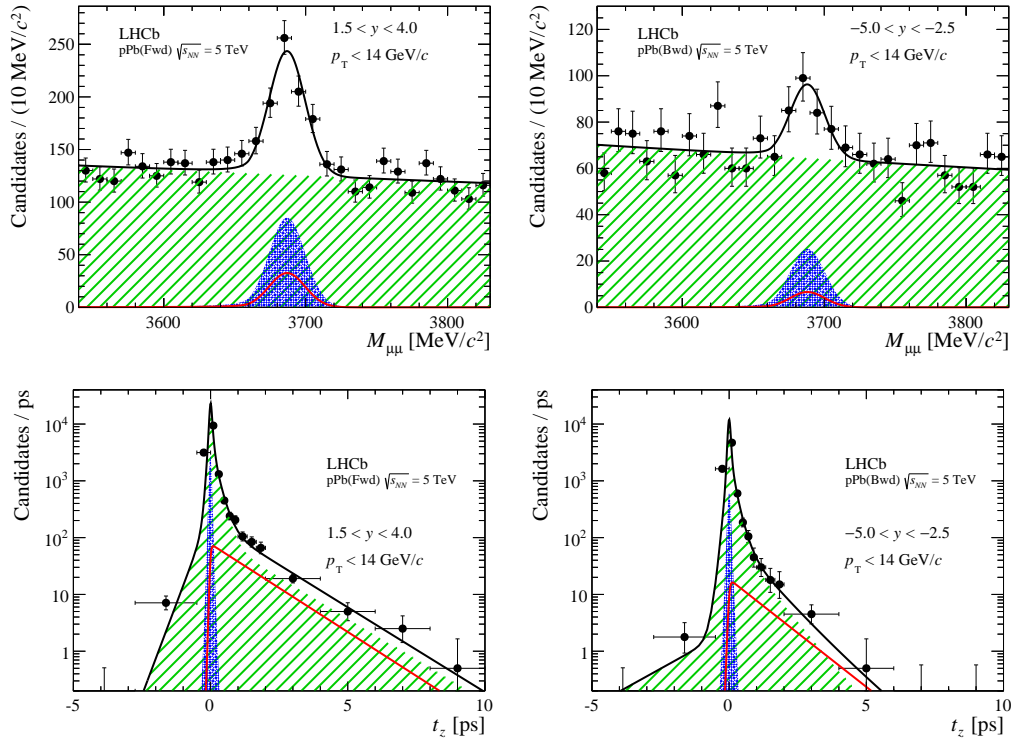


Figure 1: Projections of the fit results to (top) the dimuon invariant mass $M_{\mu\mu}$ and (bottom) the pseudo proper decay time t_z in (left) p Pb forward and (right) backward data. In all plots the total fitted function is shown by the (black) solid line, the combinatorial background component is shown as the (green) hatched area, the prompt signal component by the (blue) shaded area, and the b -component by the (red) light solid line.

5 Systematic uncertainties

Several sources of systematic uncertainties affecting the production cross-section measurements are discussed in the following and summarised in Table 1.

The uncertainty on the muon track reconstruction efficiency is studied with a data-driven tag-and-probe method, using a J/ψ sample in which one muon track is fully reconstructed while the other one is reconstructed using only specific sub-detectors [40]. Taking into account the difference of the track multiplicity distribution between data and simulation, the total uncertainty is found to be 1.5%.

The uncertainty due to the muon identification efficiency is assigned to be 1.3% for both the forward and backward samples as obtained in the J/ψ analysis in p Pb collisions [19]. It is estimated using J/ψ candidates reconstructed with one muon identified by the muon system and the other identified by selecting a track depositing the energy of a minimum-ionising particle in the calorimeters.

The trigger efficiency is determined from data using a sample unbiased with respect to the trigger decision. The corresponding uncertainty of 1.9% is taken as the systematic

Table 1: Summary of the relative systematic uncertainties on cross-section measurements (%).

Source	Forward			Backward		
	prompt	from b	inclusive	prompt	from b	inclusive
<i>Correlated between bins</i>						
Track reconstruction	1.5	1.5	1.5	1.5	1.5	1.5
Muon identification	1.3	1.3	1.3	1.3	1.3	1.3
Trigger	1.9	1.9	1.9	1.9	1.9	1.9
Luminosity	1.9	1.9	1.9	2.1	2.1	2.1
Branching fraction	2.2	2.2	2.2	2.2	2.2	2.2
Track quality and radiative tail	1.5	1.5	1.5	1.5	1.5	1.5
Mass fit	3.8 – 6.9	0.3 – 3.9	3.2 – 8.2	9.2 – 10	16 – 20	3.0 – 5.4
<i>Uncorrelated between bins</i>						
Multiplicity reweighting	0.7	0.7	0.7	1.7	1.7	1.7
Simulation kinematics	0.6 – 10	0.4 – 10	0.2 – 9.8	1.4	2.4	0.7 – 23
t_z fit	1.6 – 12	0.3 – 92	0.1 – 18	1.4 – 7.8	8.5 – 29	0.1 – 17

uncertainty due to the trigger efficiency.

To estimate the uncertainty due to reweighting the track multiplicity in simulation, the efficiency is calculated without reweighting. The difference between cross-sections calculated with these two efficiencies is considered as the systematic uncertainty, which is less than 0.7% in the forward sample, and about 1.7% in the backward sample.

The possible difference of the p_T and y spectra inside each kinematic bin between data and simulation can introduce a systematic uncertainty. To estimate the size of this effect the acceptance and reconstruction efficiencies have been checked by doubling the number of bins in p_T or in y . The difference from the nominal binning scheme is taken as systematic uncertainty, which is 0.2% – 10% (0.7% – 23%) in the forward (backward) sample. For the backward sample the separation into prompt $\psi(2S)$ and $\psi(2S)$ from b was not done in bins of p_T and y due to the limited sample size.

The luminosity is determined with an uncertainty of 1.9% (2.1%) for the pPb forward (backward) sample [36]. The uncertainty on the $\psi(2S) \rightarrow \mu^+\mu^-$ branching fraction is 2.2%. The combined uncertainty related to the track quality, the vertex finding and the radiative tail is estimated to be 1.5%.

The uncertainty due to modelling the invariant mass distribution is estimated by using the signal shape from simulation convolved with a Gaussian function, or by replacing the exponential function by a second-order polynomial. The maximum differences from the nominal results are taken as the systematic uncertainties due to the mass fit. To estimate the corresponding systematic uncertainty on the differential production cross-section due to the fixed mass resolution, the mass resolution is shifted by one standard deviation. It is found that this uncertainty is negligible. The uncertainty due to modelling the t_z distribution is estimated by fitting the signal sample extracted from the *sPlot* technique using the invariant mass alone as the discriminating variable.

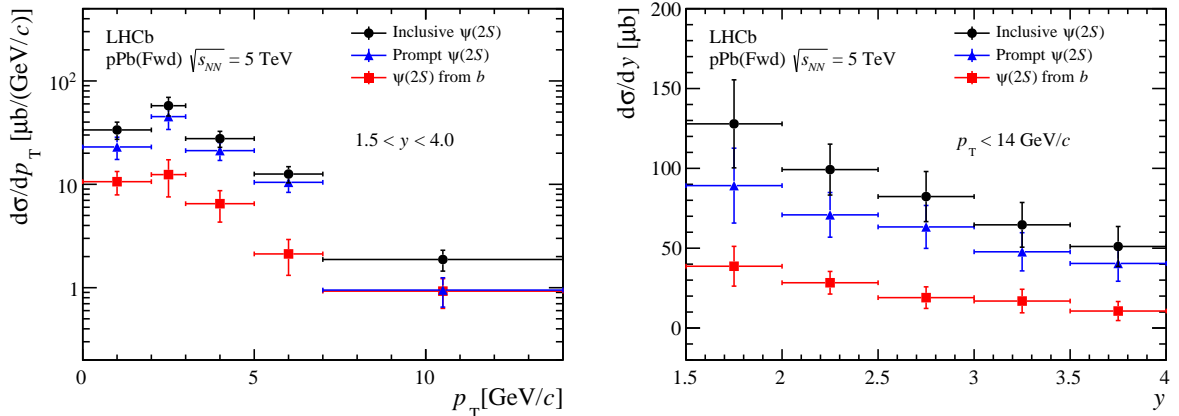


Figure 2: Differential cross-section of $\psi(2S)$ meson production as a function of (left) p_T and (right) y in p Pb forward collisions. The (black) dots represent inclusive $\psi(2S)$, the (blue) triangles indicate prompt $\psi(2S)$, and the (red) squares show $\psi(2S)$ from b . The error bars indicate the total uncertainties.

6 Results

6.1 Cross-sections

The differential cross-sections of prompt $\psi(2S)$, $\psi(2S)$ from b and inclusive $\psi(2S)$ in the p Pb forward region as functions of p_T and y are shown in Fig. 2. The differential cross-sections of inclusive $\psi(2S)$ in the p Pb backward region as functions of p_T and y are shown in Fig. 3. As stated in Sect. 5, for the differential production cross-section in the backward data sample, no attempt is made to separate prompt $\psi(2S)$ and $\psi(2S)$ from b due to the small statistics. However, these two components are separated for the integrated production cross-sections. All these cross-sections decrease with increasing $|y|$.

The integrated production cross-sections for prompt $\psi(2S)$, $\psi(2S)$ from b , and their sum representing inclusive $\psi(2S)$, are given in Table 2. To determine the forward-backward production ratio R_{FB} , the integrated production cross-sections in the common rapidity region, $2.5 < |y| < 4.0$, are also given in the table.

The production cross-sections, $\sigma(b\bar{b})$, of the $b\bar{b}$ pair can be obtained from

$$\sigma(b\bar{b}) = \sigma(\psi(2S) \text{ from } b)/2f_{b \rightarrow \psi(2S)} = \sigma(J/\psi \text{ from } b)/2f_{b \rightarrow J/\psi}, \quad (5)$$

where $f_{b \rightarrow \psi(2S)}$ ($f_{b \rightarrow J/\psi}$) indicates the production fraction of $b \rightarrow \psi(2S)X$ ($b \rightarrow J/\psi X$). The world average values are $f_{b \rightarrow J/\psi} = (1.16 \pm 0.10) \times 10^{-2}$ and $f_{b \rightarrow \psi(2S)} = (2.83 \pm 0.29) \times 10^{-3}$ [35]. The production cross-sections $\sigma(b\bar{b})$ obtained from the results of J/ψ and $\psi(2S)$ from b are shown in Table 3. The results of the $b\bar{b}$ cross-sections obtained from $\psi(2S)$ from b are consistent with those from J/ψ from b .

In the combination of the results the partial correlation between $f_{b \rightarrow \psi(2S)}$ and $f_{b \rightarrow J/\psi}$ is taken into account. The systematic uncertainties due to the muon identification, the

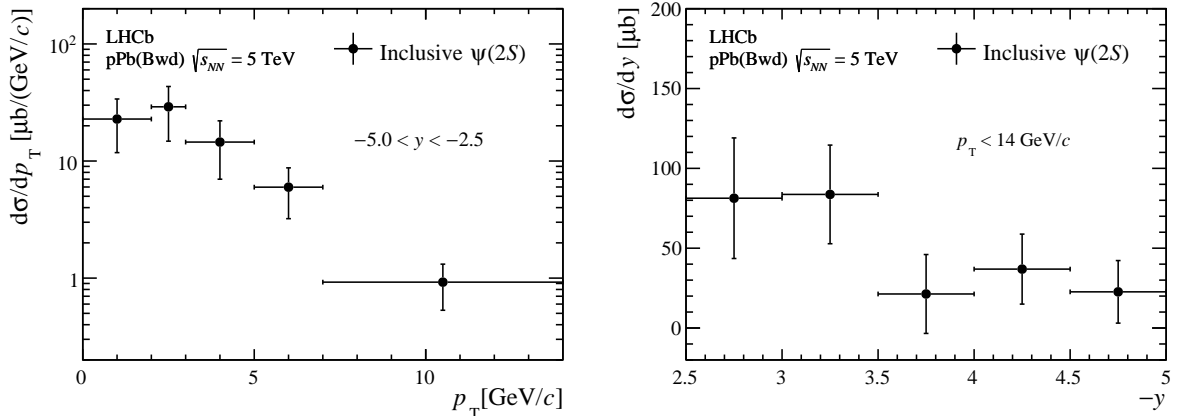


Figure 3: Differential cross-section of $\psi(2S)$ meson production as a function of (left) p_T and (right) y in $p\text{Pb}$ backward collisions. The error bars indicate the total uncertainties.

tracking efficiency, and the track quality are considered to be fully correlated. The systematic uncertainties due to the luminosities are partially correlated. The averaged results are also shown in Table 3.

6.2 Cold nuclear matter effects

Cold nuclear matter effects on $\psi(2S)$ mesons can be studied with the production cross-sections obtained in the previous section. As defined in Eq. 2, the forward-backward production ratio, R_{FB} , can be determined with the cross-sections in the common rapidity range ($2.5 < |y| < 4.0$). The results are

$$R_{\text{FB}}(p_T < 14 \text{ GeV}/c, 2.5 < |y| < 4.0) = \begin{cases} 0.93 \pm 0.29 \pm 0.08, & \text{inclusive,} \\ 0.86 \pm 0.29 \pm 0.10, & \text{prompt,} \\ 1.55 \pm 0.84 \pm 0.59, & \text{from } b, \end{cases}$$

Table 2: Integrated production cross-sections for prompt $\psi(2S)$, $\psi(2S)$ from b , and inclusive $\psi(2S)$ in the forward region and the backward region. The p_T range is $p_T < 14 \text{ GeV}/c$. The first uncertainty is statistical and the second is systematic.

	prompt [μb]	from b [μb]	inclusive [μb]
Forward ($+1.5 < y < +4.0$)	$138 \pm 17 \pm 8$	$53.7 \pm 7.9 \pm 3.6$	$192 \pm 19 \pm 10$
Backward ($-5.0 < y < -2.5$)	$93 \pm 25 \pm 10$	$20.2 \pm 8.0 \pm 4.3$	$113 \pm 26 \pm 11$
Forward ($+2.5 < y < +4.0$)	$65 \pm 10 \pm 6$	$21.4 \pm 4.5 \pm 1.1$	$86 \pm 11 \pm 7$
Backward ($-4.0 < y < -2.5$)	$76 \pm 23 \pm 10$	$13.8 \pm 6.9 \pm 5.7$	$90 \pm 24 \pm 12$

Table 3: Production cross-sections $\sigma(b\bar{b})$ of $b\bar{b}$ pairs in $p\text{Pb}$ collisions obtained from the production cross-sections of J/ψ and $\psi(2S)$ from b . The superscript ψ denotes J/ψ or $\psi(2S)$. The first uncertainties are statistical, the second are systematic, and the third are due to the production branching fractions. The last row gives the averaged results, with the first uncertainty uncorrelated and the second correlated.

	$\sigma_{\text{Fwd}}(b\bar{b})$ [mb] ($p_{\text{T}}^{\psi} < 14 \text{ GeV}/c, 1.5 < y^{\psi} < 4.0$)	$\sigma_{\text{Bwd}}(b\bar{b})$ [mb] ($p_{\text{T}}^{\psi} < 14 \text{ GeV}/c, -5.0 < y^{\psi} < -2.5$)
$\psi(2S)$	$9.49 \pm 1.40 \pm 0.64 \pm 0.97$	$3.57 \pm 1.41 \pm 0.76 \pm 0.37$
J/ψ	$7.16 \pm 0.18 \pm 0.40 \pm 0.62$	$5.09 \pm 0.29 \pm 0.53 \pm 0.44$
Averaged	$7.43 \pm 0.56(\text{uncorr}) \pm 0.49(\text{corr})$	$4.87 \pm 0.62(\text{uncorr}) \pm 0.32(\text{corr})$

where the first uncertainties are statistical and the second systematic. The ratios R_{FB} for inclusive $\psi(2S)$ production as functions of y and p_{T} are shown in Fig. 4. For comparison, the plots also show the results for inclusive J/ψ production [19] and the theoretical predictions for $\psi(2S)$ [3–5]. The uncertainties for the theoretical predictions are obtained by taking into account minimum and maximum nuclear shadowing effects, with many of them cancelling in the ratios. Calculations in Ref. [3] are based on the Leading Order Colour Singlet Model (LO CSM) [41, 42], taking into account the modification effects of the gluon distribution function in nuclei with the parameterisation EPS09 [2] or nDSg [43]. The next-to-leading order Colour Evaporation Model (NLO CEM) [44] is used in Ref. [5], considering parton shadowing with the EPS09 parameterisation. Reference [4] provides theoretical predictions of a coherent parton energy loss effect both in initial and final states, with or without additional parton shadowing effects according to EPS09. The single free parameter q_0 in this model is 0.055 (0.075) GeV^2/fm when parton shadowing in the EPS09 parameterisation is (not) taken into account. Within uncertainties the measurements agree with all these calculations.

To obtain the nuclear modification factor $R_{p\text{Pb}}$, the $\psi(2S)$ production cross-section in pp collisions at 5 TeV is needed, which is not yet available. However, it is reasonable to assume that

$$\frac{\sigma_{pp}^{J/\psi}(5 \text{ TeV})}{\sigma_{pp}^{\psi(2S)}(5 \text{ TeV})} = \frac{\sigma_{pp}^{J/\psi}(7 \text{ TeV})}{\sigma_{pp}^{\psi(2S)}(7 \text{ TeV})}, \quad (6)$$

where σ_{pp} indicates the production cross-section of J/ψ or $\psi(2S)$ in pp collisions. The systematic uncertainty due to this assumption is taken to be negligible compared with the statistical uncertainties in this analysis. The ratio R of nuclear matter effects between $\psi(2S)$ and J/ψ can then be determined as

$$R \equiv \frac{R_{p\text{Pb}}^{\psi(2S)}}{R_{p\text{Pb}}^{J/\psi}} = \frac{\sigma_{p\text{Pb}}^{\psi(2S)}(5 \text{ TeV})}{\sigma_{p\text{Pb}}^{J/\psi}(5 \text{ TeV})} \times \frac{\sigma_{pp}^{J/\psi}(5 \text{ TeV})}{\sigma_{pp}^{\psi(2S)}(5 \text{ TeV})} = \frac{\sigma_{p\text{Pb}}^{\psi(2S)}(5 \text{ TeV})}{\sigma_{p\text{Pb}}^{J/\psi}(5 \text{ TeV})} \times \frac{\sigma_{pp}^{J/\psi}(7 \text{ TeV})}{\sigma_{pp}^{\psi(2S)}(7 \text{ TeV})}, \quad (7)$$

where $R_{p\text{Pb}}^{\psi(2S)}$ and $R_{p\text{Pb}}^{J/\psi}$ are the nuclear modification factors for $\psi(2S)$ and J/ψ . The ratio

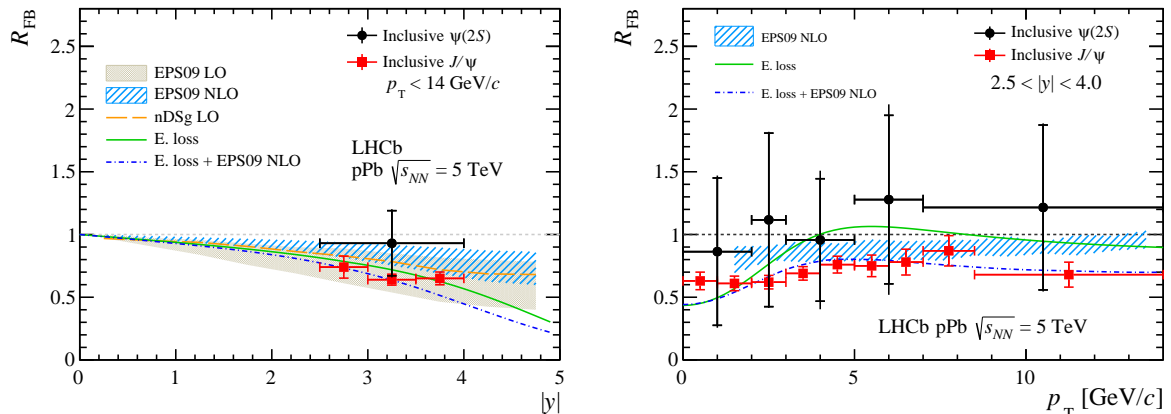


Figure 4: Forward-backward production ratios R_{FB} as functions of (left) $|y|$ and (right) p_T for inclusive $\psi(2S)$ mesons, together with inclusive J/ψ results [19] and the theoretical predictions [3–5], only some of which are available for $|y|$. The inner error bars (delimited by the horizontal lines) show the statistical uncertainties; the outer ones show the statistical and systematic uncertainties added in quadrature.

R indicates whether there is relative suppression between $\psi(2S)$ and J/ψ production in the collisions. If R is less than unity, it suggests that the suppression of $\psi(2S)$ mesons due to nuclear matter effects in pPb collisions is stronger than that of J/ψ mesons. Using previous LHCb measurements [19, 33, 45], the values of R for prompt $\psi(2S)$, $\psi(2S)$ from b and inclusive $\psi(2S)$ are calculated. The results are shown in Fig. 5, together with those from ALICE [21] and PHENIX [18]. The LHCb measurement is consistent with ALICE, which is in a comparable kinematic range. All results suggest a stronger suppression for prompt $\psi(2S)$ mesons than that for prompt J/ψ mesons.

The nuclear modification factor of $\psi(2S)$, $R_{pPb}^{\psi(2S)}$, can be expressed in terms of $R_{pPb}^{J/\psi}$ and R

$$R_{pPb}^{\psi(2S)} = R_{pPb}^{J/\psi} \times R. \quad (8)$$

The nuclear modification factor $R_{pPb}^{J/\psi}$ was determined in a previous measurement [19]. The result for inclusive $\psi(2S)$ is shown in Fig. 6. For comparison, the inclusive J/ψ result from previous measurements [19] and the result from ALICE [21] are also shown in the plot. The LHCb measurement is consistent with ALICE. The results for prompt $\psi(2S)$ and $\psi(2S)$ from b are shown in Fig. 7, suggesting that in pPb collisions the suppression of prompt $\psi(2S)$ mesons is stronger than that of prompt J/ψ mesons. For $\psi(2S)$ from b , no conclusion can be made because of the limited sample size. Figure 7 also shows several theoretical predictions [3–5, 46], where only those from Ref. [46] are available for $\psi(2S)$ from b . For prompt $\psi(2S)$, stronger suppression is seen in the data than expected by the theoretical calculations. Final-state effects, such as the interaction of the $c\bar{c}$ pair with the dense medium created in the collisions, could be involved [47].

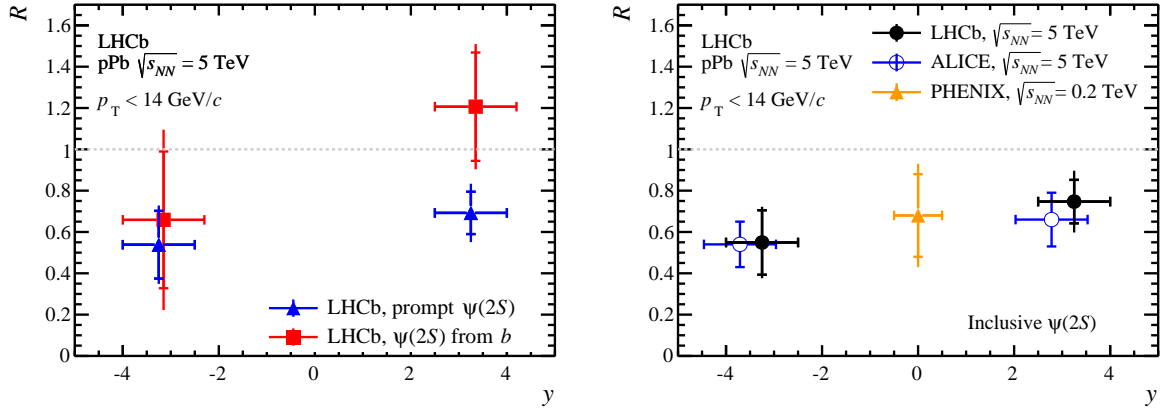


Figure 5: Ratio (left) between nuclear modification factors of $\psi(2S)$ and J/ψ as a function of y for prompt $\psi(2S)$ mesons and $\psi(2S)$ from b . The blue triangles represent prompt $\psi(2S)$ and the red rectangles indicate $\psi(2S)$ from b . Ratio (right) between nuclear modification factors of $\psi(2S)$ and J/ψ as a function of y for inclusive $\psi(2S)$ mesons. The black dots show the LHCb result, the hollow circles indicate the ALICE result, and the brown triangle is the PHENIX result at 0.2 TeV. The inner error bars (delimited by the horizontal lines) show the statistical uncertainties; the outer ones show the statistical and systematic uncertainties added in quadrature.

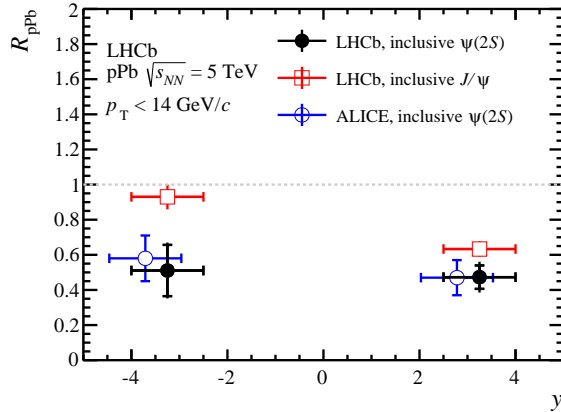


Figure 6: Nuclear modification factor R_{pPb} as a function of y for inclusive $\psi(2S)$ and J/ψ mesons. The black dots represent the $\psi(2S)$ result, the red squares indicate the J/ψ result, and the blue hollow circles show the ALICE result for $\psi(2S)$. The inner error bars (delimited by the horizontal lines) show the statistical uncertainties; the outer ones show the statistical and systematic uncertainties added in quadrature.

7 Conclusions

The production cross-sections of prompt $\psi(2S)$ mesons and those from b -hadron decays are studied in pPb collisions with the LHCb detector. The nucleon-nucleon centre-of-mass

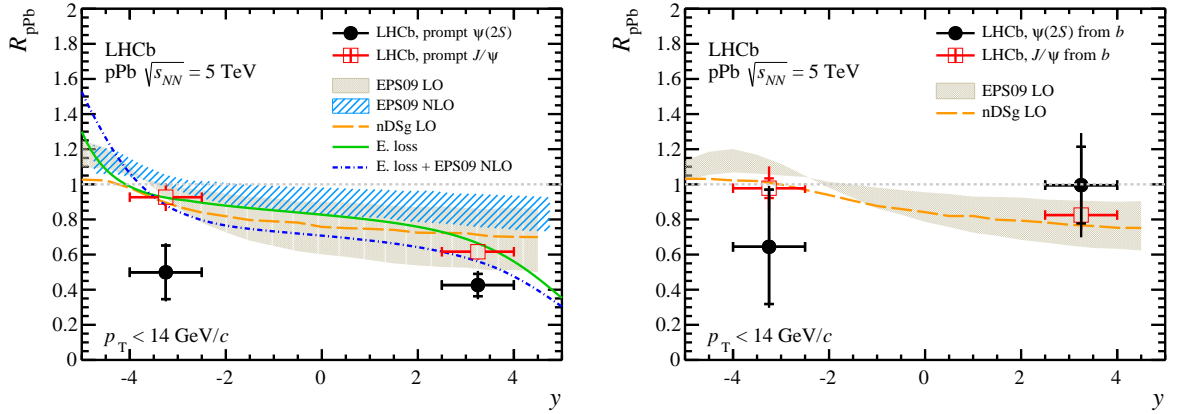


Figure 7: Nuclear modification factor $R_{p\text{Pb}}$ as a function of y for (left) prompt $\psi(2S)$ and (right) $\psi(2S)$ from b , together with the theoretical predictions from (yellow dashed line and brown band) Refs. [3, 46], (blue band) Ref. [5], and (green solid and blue dash-dotted lines) Ref. [4], where only those from Ref. [46] are available for $\psi(2S)$ from b . The inner error bars (delimited by the horizontal lines) show the statistical uncertainties; the outer ones show the statistical and systematic uncertainties added in quadrature.

energy in the collisions is $\sqrt{s_{NN}} = 5 \text{ TeV}$. The measurement is performed as a function of the transverse momentum and rapidity of $\psi(2S)$ mesons in the region $p_T < 14 \text{ GeV}/c$ and $1.5 < y < 4.0$ (forward) and $-5.0 < y < -2.5$ (backward). The $b\bar{b}$ production cross-sections in $p\text{Pb}$ collisions are extracted using the results of $\psi(2S)$ from b and J/ψ from b . The forward-backward production ratio R_{FB} is determined separately for prompt $\psi(2S)$ mesons and those from b -hadron decays. These results show agreement within uncertainties with available theoretical predictions. The nuclear modification factor $R_{p\text{Pb}}$ is also determined separately for prompt $\psi(2S)$ mesons and $\psi(2S)$ from b . These results show that prompt $\psi(2S)$ mesons are significantly more suppressed than prompt J/ψ mesons in the backward region; the results are not well described by theoretical predictions based on shadowing and energy loss mechanisms.

Acknowledgements

We express our gratitude to our colleagues in the CERN accelerator departments for the excellent performance of the LHC. We thank the technical and administrative staff at the LHCb institutes. We acknowledge support from CERN and from the national agencies: CAPES, CNPq, FAPERJ and FINEP (Brazil); NSFC (China); CNRS/IN2P3 (France); BMBF, DFG and MPG (Germany); INFN (Italy); FOM and NWO (The Netherlands); MNiSW and NCN (Poland); MEN/IFA (Romania); MinES and FANO (Russia); MinECo (Spain); SNSF and SER (Switzerland); NASU (Ukraine); STFC (United Kingdom); NSF (USA). We acknowledge the computing resources that are provided by CERN, IN2P3 (France), KIT and DESY (Germany), INFN (Italy), SURF (The Netherlands), PIC (Spain), GridPP (United Kingdom), RRCKI and Yandex LLC (Russia), CSCS (Switzerland), IFIN-HH (Romania), CBPF (Brazil), PL-GRID (Poland) and OSC (USA). We are indebted to the communities behind the multiple open source software packages on which we depend. Individual groups or members have received support from AvH Foundation (Germany), EPLANET, Marie Skłodowska-Curie Actions and ERC (European Union), Conseil Général de Haute-Savoie, Labex ENIGMASS and OCEVU, Région Auvergne (France), RFBR and Yandex LLC (Russia), GVA, XuntaGal and GENCAT (Spain), The Royal Society, Royal Commission for the Exhibition of 1851 and the Leverhulme Trust (United Kingdom).

References

- [1] T. Matsui and H. Satz, *J/ψ suppression by quark-gluon plasma formation*, Phys. Lett. **B178** (1986) 416.
- [2] K. J. Eskola, H. Paukkunen, and C. A. Salgado, *EPS09 – a new generation of NLO and LO nuclear parton distribution functions*, JHEP **04** (2009) 065, [arXiv:0902.4154](#).
- [3] E. G. Ferreiro, F. Fleuret, J. P. Lansberg, and A. Rakotozafindrabe, *Impact of the nuclear modification of the gluon densities on J/ψ production in pPb collisions at $\sqrt{s_{NN}} = 5$ TeV*, Phys. Rev. **C88** (2013) 047901, [arXiv:1305.4569](#).
- [4] F. Arleo and S. Peigné, *Heavy-quarkonium suppression in p-A collisions from parton energy loss in cold QCD matter*, JHEP **03** (2013) 122, [arXiv:1212.0434](#).
- [5] J. L. Albacete *et al.*, *Predictions for p+Pb collisions at $\sqrt{s_{NN}} = 5$ TeV*, Int. J. Mod. Phys. **E22** (2013) 1330007, [arXiv:1301.3395](#).
- [6] A. Adeluyi and T. Nguyen, *Coherent photoproduction of ψ and Υ mesons in ultraperipheral pPb and PbPb collisions at the CERN Large Hadron Collider at $\sqrt{s_{NN}} = 5$ TeV and $\sqrt{s_{NN}} = 2.76$ TeV*, Phys. Rev. **C87** (2013) 027901, [arXiv:1302.4288](#).
- [7] G. A. Chirilli, B.-W. Xiao, and F. Yuan, *Inclusive hadron productions in pA collisions*, Phys. Rev. **D86** (2012) 054005, [arXiv:1203.6139](#).

- [8] G. A. Chirilli, *High-energy QCD factorization from DIS to pA collisions*, Int. J. Mod. Phys. Conf. Ser. **20** (2012) 200, [arXiv:1209.1614](#).
- [9] F. Arleo, R. Kolevatov, S. Peigné, and M. Rustamova, *Centrality and p_{\perp} dependence of J/ψ suppression in proton-nucleus collisions from parton energy loss*, JHEP **05** (2013) 155, [arXiv:1304.0901](#).
- [10] FNAL E866/NuSea collaboration, M. J. Leitch *et al.*, *Measurement of differences between J/ψ and ψ' suppression in p-A collisions*, Phys. Rev. Lett. **84** (2000) 3256, [arXiv:nucl-ex/9909007](#).
- [11] NA50 collaboration, B. Alessandro *et al.*, *J/ψ and ψ' production and their normal nuclear absorption in proton-nucleus collisions at 400 GeV*, Eur. Phys. J. **C48** (2006) 329, [arXiv:nucl-ex/0612012](#).
- [12] HERA-B collaboration, I. Abt *et al.*, *A Measurement of the ψ' to J/ψ production ratio in 920 GeV proton-nucleus interactions*, Eur. Phys. J. **C49** (2007) 545, [arXiv:hep-ex/0607046](#).
- [13] HERA-B collaboration, I. Abt *et al.*, *Kinematic distributions and nuclear effects of J/ψ production in 920 GeV fixed-target proton-nucleus collisions*, Eur. Phys. J. **C60** (2009) 525, [arXiv:0812.0734](#).
- [14] BRAHMS collaboration, I. Arsene *et al.*, *Evolution of the nuclear modification factors with rapidity and centrality in $d + Au$ collisions at $\sqrt{s_{NN}} = 200$ GeV*, Phys. Rev. Lett. **93** (2004) 242303, [arXiv:nucl-ex/0403005](#).
- [15] PHENIX collaboration, S. S. Adler *et al.*, *Nuclear modification factors for hadrons at forward and backward rapidities in deuteron-gold collisions at $\sqrt{s_{NN}} = 200$ GeV*, Phys. Rev. Lett. **94** (2005) 082302, [arXiv:nucl-ex/0411054](#).
- [16] PHENIX collaboration, A. Adare *et al.*, *Cold nuclear matter effects on J/ψ yields as a function of rapidity and nuclear geometry in $d + Au$ collisions at $\sqrt{s_{NN}} = 200$ GeV*, Phys. Rev. Lett. **107** (2011) 142301, [arXiv:1010.1246](#).
- [17] PHENIX collaboration, A. Adare *et al.*, *$\Upsilon(1S + 2S + 3S)$ production in $d+Au$ and $p + p$ collisions at $\sqrt{s_{NN}} = 200$ GeV and cold-nuclear matter effects*, Phys. Rev. **C87** (2013) 044909, [arXiv:1211.4017](#).
- [18] PHENIX collaboration, A. Adare *et al.*, *Nuclear modification of ψ' , χ_c , and J/ψ production in $d+Au$ collisions at $\sqrt{s_{NN}} = 200$ GeV*, Phys. Rev. Lett. **111** (2013) 202301, [arXiv:1305.5516](#).
- [19] LHCb collaboration, R. Aaij *et al.*, *Study of J/ψ production and cold nuclear matter effects in pPb collisions at $\sqrt{s_{NN}} = 5$ TeV*, JHEP **02** (2014) 072, [arXiv:1308.6729](#).

- [20] LHCb collaboration, R. Aaij *et al.*, *Study of Υ production and cold nuclear effects in p -Pb collisions at $\sqrt{s_{NN}} = 5$ TeV*, JHEP **07** (2014) 094, [arXiv:1405.5152](#).
- [21] ALICE collaboration, B. B. Abelev *et al.*, *Suppression of $\psi(2S)$ production in p -Pb collisions at $\sqrt{s_{NN}} = 5.02$ TeV*, JHEP **12** (2014) 073, [arXiv:1405.3796](#).
- [22] R. Vogt, *Are the J/ψ and χ_c A dependencies the same?*, Nucl. Phys. **A700** (2002) 539, [arXiv:hep-ph/0107045](#).
- [23] B. Z. Kopeliovich and B. G. Zakharov, *Quantum effects and color transparency in charmonium photoproduction on nuclei*, Phys. Rev. **D44** (1991) 3466.
- [24] D. C. McGlinchey, A. D. Frawley, and R. Vogt, *Impact parameter dependence of the nuclear modification of J/ψ production in d +Au collisions at $\sqrt{s_{NN}} = 200$ GeV*, Phys. Rev. **C87** (2013) 054910, [arXiv:1208.2667](#).
- [25] LHCb collaboration, A. A. Alves Jr. *et al.*, *The LHCb detector at the LHC*, JINST **3** (2008) S08005.
- [26] LHCb collaboration, R. Aaij *et al.*, *LHCb detector performance*, Int. J. Mod. Phys. **A30** (2015) 1530022, [arXiv:1412.6352](#).
- [27] T. Sjöstrand, S. Mrenna, and P. Skands, *PYTHIA 6.4 physics and manual*, JHEP **05** (2006) 026, [arXiv:hep-ph/0603175](#).
- [28] I. Belyaev *et al.*, *Handling of the generation of primary events in Gauss, the LHCb simulation framework*, J. Phys. Conf. Ser. **331** (2011) 032047.
- [29] D. J. Lange, *The EvtGen particle decay simulation package*, Nucl. Instrum. Meth. **A462** (2001) 152.
- [30] P. Golonka and Z. Was, *PHOTOS Monte Carlo: A precision tool for QED corrections in Z and W decays*, Eur. Phys. J. **C45** (2006) 97, [arXiv:hep-ph/0506026](#).
- [31] Geant4 collaboration, J. Allison *et al.*, *Geant4 developments and applications*, IEEE Trans. Nucl. Sci. **53** (2006) 270; Geant4 collaboration, S. Agostinelli *et al.*, *Geant4: A simulation toolkit*, Nucl. Instrum. Meth. **A506** (2003) 250.
- [32] M. Clemencic *et al.*, *The LHCb simulation application, Gauss: Design, evolution and experience*, J. Phys. Conf. Ser. **331** (2011) 032023.
- [33] LHCb collaboration, R. Aaij *et al.*, *Measurement of J/ψ production in pp collisions at $\sqrt{s} = 7$ TeV*, Eur. Phys. J. **C71** (2011) 1645, [arXiv:1103.0423](#).
- [34] LHCb collaboration, R. Aaij *et al.*, *Production of J/ψ and Υ mesons in pp collisions at $\sqrt{s} = 8$ TeV*, JHEP **06** (2013) 064, [arXiv:1304.6977](#).

- [35] Particle Data Group, K. A. Olive *et al.*, *Review of particle physics*, Chin. Phys. **C38** (2014) 090001, and 2015 update.
- [36] LHCb collaboration, R. Aaij *et al.*, *Precision luminosity measurements at LHCb*, JINST **9** (2014) P12005, arXiv:1410.0149.
- [37] T. Skwarnicki, *A study of the radiative cascade transitions between the Upsilon-prime and Upsilon resonances*, PhD thesis, Institute of Nuclear Physics, Krakow, 1986, DESY-F31-86-02.
- [38] W. Qian, *J/ψ production study at the LHCb experiment*, CERN-THESIS-2010-307.
- [39] M. Pivk and F. R. Le Diberder, *sPlot: A statistical tool to unfold data distributions*, Nucl. Instrum. Meth. **A555** (2005) 356, arXiv:physics/0402083.
- [40] LHCb collaboration, R. Aaij *et al.*, *Measurement of the track reconstruction efficiency at LHCb*, JINST **10** (2015) P02007, arXiv:1408.1251.
- [41] C.-H. Chang, *Hadronic production of J/ψ associated with a gluon*, Nucl. Phys. **B172** (1980) 425.
- [42] R. Baier and R. Rückl, *Hadronic production of J/ψ and Υ: Transverse momentum distributions*, Phys. Lett. **B102** (1981) 364.
- [43] D. de Florian and R. Sassot, *Nuclear parton distributions at next-to-leading order*, Phys. Rev. **D69** (2004) 074028, arXiv:hep-ph/0311227.
- [44] M. Glück, J. F. Owens, and E. Reya, *Gluon contribution to hadronic J/ψ production*, Phys. Rev. **D17** (1978) 2324.
- [45] LHCb collaboration, R. Aaij *et al.*, *Measurement of ψ(2S) meson production in pp collisions at √s = 7 TeV*, Eur. Phys. J. **C72** (2012) 2100, arXiv:1204.1258.
- [46] Z. Conesa del Valle *et al.*, *Open-beauty production in p-Pb collisions at √s_{NN} = 5 TeV: Effect of the gluon nuclear densities*, Nucl. Phys. **A926** (2014) 236, arXiv:1402.1747.
- [47] E. G. Ferreiro, *Excited charmonium suppression in proton-nucleus collisions as a consequence of comovers*, Phys. Lett. **B749** (2015) 98, arXiv:1411.0549.

LHCb collaboration

R. Aaij³⁹, C. Abellán Beteta⁴¹, B. Adeva³⁸, M. Adinolfi⁴⁷, A. Affolder⁵³, Z. Ajaltouni⁵, S. Akar⁶, J. Albrecht¹⁰, F. Alessio³⁹, M. Alexander⁵², S. Ali⁴², G. Alkhazov³¹, P. Alvarez Cartelle⁵⁴, A.A. Alves Jr⁵⁸, S. Amato², S. Amerio²³, Y. Amhis⁷, L. An^{3,40}, L. Anderlini¹⁸, G. Andreassi⁴⁰, M. Andreotti^{17,g}, J.E. Andrews⁵⁹, R.B. Appleby⁵⁵, O. Aquines Gutierrez¹¹, F. Archilli³⁹, P. d'Argent¹², A. Artamonov³⁶, M. Artuso⁶⁰, E. Aslanides⁶, G. Auriemma^{26,n}, M. Baalouch⁵, S. Bachmann¹², J.J. Back⁴⁹, A. Badalov³⁷, C. Baesso⁶¹, W. Baldini^{17,39}, R.J. Barlow⁵⁵, C. Barschel³⁹, S. Barsuk⁷, W. Barter³⁹, V. Batozskaya²⁹, V. Battista⁴⁰, A. Bay⁴⁰, L. Beaucourt⁴, J. Beddow⁵², F. Bedeschi²⁴, I. Bediaga¹, L.J. Bel⁴², V. Bellee⁴⁰, N. Belloli^{21,k}, I. Belyaev³², E. Ben-Haim⁸, G. Bencivenni¹⁹, S. Benson³⁹, J. Benton⁴⁷, A. Berezhnoy³³, R. Bernet⁴¹, A. Bertolin²³, F. Betti¹⁵, M.-O. Bettler³⁹, M. van Beuzekom⁴², S. Bifani⁴⁶, P. Billoir⁸, T. Bird⁵⁵, A. Birnkraut¹⁰, A. Bizzeti^{18,i}, T. Blake⁴⁹, F. Blanc⁴⁰, J. Blouw¹¹, S. Blusk⁶⁰, V. Bocci²⁶, A. Bondar³⁵, N. Bondar^{31,39}, W. Bonivento¹⁶, A. Borgheresi^{21,k}, S. Borghi⁵⁵, M. Borisyak⁶⁶, M. Borsato³⁸, T.J.V. Bowcock⁵³, E. Bowen⁴¹, C. Bozzi^{17,39}, S. Braun¹², M. Britsch¹², T. Britton⁶⁰, J. Brodzicka⁵⁵, N.H. Brook⁴⁷, E. Buchanan⁴⁷, C. Burr⁵⁵, A. Bursche², J. Buytaert³⁹, S. Cadeddu¹⁶, R. Calabrese^{17,g}, M. Calvi^{21,k}, M. Calvo Gomez^{37,p}, P. Campana¹⁹, D. Campora Perez³⁹, L. Capriotti⁵⁵, A. Carbone^{15,e}, G. Carboni^{25,l}, R. Cardinale^{20,j}, A. Cardini¹⁶, P. Carniti^{21,k}, L. Carson⁵¹, K. Carvalho Akiba², G. Casse⁵³, L. Cassina^{21,k}, L. Castillo Garcia⁴⁰, M. Cattaneo³⁹, Ch. Cauet¹⁰, G. Cavallero²⁰, R. Cenci^{24,t}, M. Charles⁸, Ph. Charpentier³⁹, M. Chefdeville⁴, S. Chen⁵⁵, S.-F. Cheung⁵⁶, N. Chiapolini⁴¹, M. Chrzaszcz^{41,27}, X. Cid Vidal³⁹, G. Ciezarek⁴², P.E.L. Clarke⁵¹, M. Clemencic³⁹, H.V. Cliff⁴⁸, J. Closier³⁹, V. Coco³⁹, J. Cogan⁶, E. Cogneras⁵, V. Cogoni^{16,f}, L. Cojocariu³⁰, G. Collazuol^{23,r}, P. Collins³⁹, A. Comerma-Montells¹², A. Contu³⁹, A. Cook⁴⁷, M. Coombes⁴⁷, S. Coquereau⁸, G. Corti³⁹, M. Corvo^{17,g}, B. Couturier³⁹, G.A. Cowan⁵¹, D.C. Craik⁵¹, A. Crocombe⁴⁹, M. Cruz Torres⁶¹, S. Cunliffe⁵⁴, R. Currie⁵⁴, C. D'Ambrosio³⁹, E. Dall'Occo⁴², J. Dalseno⁴⁷, P.N.Y. David⁴², A. Davis⁵⁸, O. De Aguiar Francisco², K. De Bruyn⁶, S. De Capua⁵⁵, M. De Cian¹², J.M. De Miranda¹, L. De Paula², P. De Simone¹⁹, C.-T. Dean⁵², D. Decamp⁴, M. Deckenhoff¹⁰, L. Del Buono⁸, N. Déleage⁴, M. Demmer¹⁰, D. Derkach⁶⁶, O. Deschamps⁵, F. Dettori³⁹, B. Dey²², A. Di Canto³⁹, F. Di Ruscio²⁵, H. Dijkstra³⁹, S. Donleavy⁵³, F. Dordei³⁹, M. Dorigo⁴⁰, A. Dosil Suárez³⁸, A. Dovbnya⁴⁴, K. Dreimanis⁵³, L. Dufour⁴², G. Dujany⁵⁵, K. Dungs³⁹, P. Durante³⁹, R. Dzhelyadin³⁶, A. Dziurda²⁷, A. Dzyuba³¹, S. Easo^{50,39}, U. Egede⁵⁴, V. Egorychev³², S. Eidelman³⁵, S. Eisenhardt⁵¹, U. Eitschberger¹⁰, R. Ekelhof¹⁰, L. Eklund⁵², I. El Rifai⁵, Ch. Elsasser⁴¹, S. Ely⁶⁰, S. Esen¹², H.M. Evans⁴⁸, T. Evans⁵⁶, A. Falabella¹⁵, C. Färber³⁹, N. Farley⁴⁶, S. Farry⁵³, R. Fay⁵³, D. Fazzini^{21,k}, D. Ferguson⁵¹, V. Fernandez Albor³⁸, F. Ferrari¹⁵, F. Ferreira Rodrigues¹, M. Ferro-Luzzi³⁹, S. Filippov³⁴, M. Fiore^{17,39,g}, M. Fiorini^{17,g}, M. Firlej²⁸, C. Fitzpatrick⁴⁰, T. Fiutowski²⁸, F. Fleuret^{7,b}, K. Fohl³⁹, P. Fol⁵⁴, M. Fontana¹⁶, F. Fontanelli^{20,j}, D. C. Forshaw⁶⁰, R. Forty³⁹, M. Frank³⁹, C. Frei³⁹, M. Frosini¹⁸, J. Fu²², E. Furfaro^{25,l}, A. Gallas Torreira³⁸, D. Galli^{15,e}, S. Gallorini²³, S. Gambetta⁵¹, M. Gandelman², P. Gandini⁵⁶, Y. Gao³, J. García Pardiñas³⁸, J. Garra Tico⁴⁸, L. Garrido³⁷, D. Gascon³⁷, C. Gaspar³⁹, L. Gavardi¹⁰, G. Gazzoni⁵, D. Gerick¹², E. Gersabeck¹², M. Gersabeck⁵⁵, T. Gershon⁴⁹, Ph. Ghez⁴, S. Gianì⁴⁰, V. Gibson⁴⁸, O.G. Girard⁴⁰, L. Giubega³⁰, V.V. Gligorov³⁹, C. Göbel⁶¹, D. Golubkov³², A. Golutvin^{54,39}, A. Gomes^{1,a}, C. Gotti^{21,k}, M. Grabalosa Gándara⁵, R. Graciani Diaz³⁷, L.A. Granado Cardoso³⁹, E. Graugés³⁷, E. Graverini⁴¹, G. Graziani¹⁸, A. Grecu³⁰, P. Griffith⁴⁶, L. Grillo¹², O. Grünberg⁶⁴, B. Gui⁶⁰, E. Gushchin³⁴, Yu. Guz^{36,39}, T. Gys³⁹, T. Hadavizadeh⁵⁶, C. Hadjivasiliou⁶⁰, G. Haefeli⁴⁰,

C. Haen³⁹, S.C. Haines⁴⁸, S. Hall⁵⁴, B. Hamilton⁵⁹, X. Han¹², S. Hansmann-Menzemer¹²,
 N. Harnew⁵⁶, S.T. Harnew⁴⁷, J. Harrison⁵⁵, J. He³⁹, T. Head⁴⁰, V. Heijne⁴², A. Heister⁹,
 K. Hennessy⁵³, P. Henrard⁵, L. Henry⁸, J.A. Hernando Morata³⁸, E. van Herwijnen³⁹, M. Heß⁶⁴,
 A. Hicheur², D. Hill⁵⁶, M. Hoballah⁵, C. Hombach⁵⁵, L. Hongming⁴⁰, W. Hulsbergen⁴²,
 T. Humair⁵⁴, M. Hushchyn⁶⁶, N. Hussain⁵⁶, D. Hutchcroft⁵³, D. Hynds⁵², M. Idzik²⁸, P. Ilten⁵⁷,
 R. Jacobsson³⁹, A. Jaeger¹², J. Jalocha⁵⁶, E. Jans⁴², A. Jawahery⁵⁹, M. John⁵⁶, D. Johnson³⁹,
 C.R. Jones⁴⁸, C. Joram³⁹, B. Jost³⁹, N. Jurik⁶⁰, S. Kandybei⁴⁴, W. Kanso⁶, M. Karacson³⁹,
 T.M. Karbach^{39,†}, S. Karodia⁵², M. Kecke¹², M. Kelsey⁶⁰, I.R. Kenyon⁴⁶, M. Kenzie³⁹,
 T. Ketel⁴³, E. Khairullin⁶⁶, B. Khanji^{21,39,k}, C. Khurewathanakul⁴⁰, T. Kirn⁹, S. Klaver⁵⁵,
 K. Klimaszewski²⁹, O. Kochebina⁷, M. Kolpin¹², I. Komarov⁴⁰, R.F. Koopman⁴³,
 P. Koppenburg^{42,39}, M. Kozeiha⁵, L. Kravchuk³⁴, K. Kreplin¹², M. Krepis⁴⁹, P. Krokovny³⁵,
 F. Kruse¹⁰, W. Krzemien²⁹, W. Kucewicz^{27,o}, M. Kucharczyk²⁷, V. Kudryavtsev³⁵, A.
 K. Kuonen⁴⁰, K. Kurek²⁹, T. Kvaratskheliya³², D. Lacarrere³⁹, G. Lafferty^{55,39}, A. Lai¹⁶,
 D. Lambert⁵¹, G. Lanfranchi¹⁹, C. Langenbruch⁴⁹, B. Langhans³⁹, T. Latham⁴⁹, C. Lazzeroni⁴⁶,
 R. Le Gac⁶, J. van Leerdam⁴², J.-P. Lees⁴, R. Lefèvre⁵, A. Leflat^{33,39}, J. Lefrançois⁷,
 E. Lemos Cid³⁸, O. Leroy⁶, T. Lesiak²⁷, B. Leverington¹², Y. Li⁷, T. Likhomanenko^{66,65},
 M. Liles⁵³, R. Lindner³⁹, C. Linn³⁹, F. Lionetto⁴¹, B. Liu¹⁶, X. Liu³, D. Loh⁴⁹, I. Longstaff⁵²,
 J.H. Lopes², D. Lucchesi^{23,r}, M. Lucio Martinez³⁸, H. Luo⁵¹, A. Lupato²³, E. Luppi^{17,g},
 O. Lupton⁵⁶, A. Lusiani²⁴, F. Machefert⁷, F. Maciuc³⁰, O. Maev³¹, K. Maguire⁵⁵, S. Malde⁵⁶,
 A. Malinin⁶⁵, G. Manca⁷, G. Mancinelli⁶, P. Manning⁶⁰, A. Mapelli³⁹, J. Maratas⁵,
 J.F. Marchand⁴, U. Marconi¹⁵, C. Marin Benito³⁷, P. Marino^{24,39,t}, J. Marks¹², G. Martellotti²⁶,
 M. Martin⁶, M. Martinelli⁴⁰, D. Martinez Santos³⁸, F. Martinez Vidal⁶⁷, D. Martins Tostes²,
 L.M. Massacrier⁷, A. Massafferri¹, R. Matev³⁹, A. Mathad⁴⁹, Z. Mathe³⁹, C. Matteuzzi²¹,
 A. Mauri⁴¹, B. Maurin⁴⁰, A. Mazurov⁴⁶, M. McCann⁵⁴, J. McCarthy⁴⁶, A. McNab⁵⁵,
 R. McNulty¹³, B. Meadows⁵⁸, F. Meier¹⁰, M. Meissner¹², D. Melnychuk²⁹, M. Merk⁴²,
 A Merli^{22,u}, E. Michielin²³, D.A. Milanes⁶³, M.-N. Minard⁴, D.S. Mitzel¹², J. Molina Rodriguez⁶¹,
 I.A. Monroy⁶³, S. Monteil⁵, M. Morandin²³, P. Morawski²⁸, A. Mordà⁶, M.J. Morello^{24,t},
 J. Moron²⁸, A.B. Morris⁵¹, R. Mountain⁶⁰, F. Muheim⁵¹, D. Müller⁵⁵, J. Müller¹⁰, K. Müller⁴¹,
 V. Müller¹⁰, M. Mussini¹⁵, B. Muster⁴⁰, P. Naik⁴⁷, T. Nakada⁴⁰, R. Nandakumar⁵⁰, A. Nandi⁵⁶,
 I. Nasteva², M. Needham⁵¹, N. Neri²², S. Neubert¹², N. Neufeld³⁹, M. Neuner¹², A.D. Nguyen⁴⁰,
 C. Nguyen-Mau^{40,q}, V. Niess⁵, S. Nieswand⁹, R. Niet¹⁰, N. Nikitin³³, T. Nikodem¹²,
 A. Novoselov³⁶, D.P. O’Hanlon⁴⁹, A. Oblakowska-Mucha²⁸, V. Obraztsov³⁶, S. Ogilvy⁵²,
 O. Okhrimenko⁴⁵, R. Oldeman^{16,48,f}, C.J.G. Onderwater⁶⁸, B. Osorio Rodrigues¹,
 J.M. Otalora Goicochea², A. Otto³⁹, P. Owen⁵⁴, A. Oyanguren⁶⁷, A. Palano^{14,d}, F. Palombo^{22,u},
 M. Palutan¹⁹, J. Panman³⁹, A. Papanestis⁵⁰, M. Pappagallo⁵², L.L. Pappalardo^{17,g},
 C. Pappenheimer⁵⁸, W. Parker⁵⁹, C. Parkes⁵⁵, G. Passaleva¹⁸, G.D. Patel⁵³, M. Patel⁵⁴,
 C. Patrignani^{20,j}, A. Pearce^{55,50}, A. Pellegrino⁴², G. Penso^{26,m}, M. Pepe Altarelli³⁹,
 S. Perazzini^{15,e}, P. Perret⁵, L. Pescatore⁴⁶, K. Petridis⁴⁷, A. Petrolini^{20,j}, M. Petruzzo²²,
 E. Picatoste Olloqui³⁷, B. Pietrzyk⁴, M. Pikies²⁷, D. Pinci²⁶, A. Pistone²⁰, A. Piucci¹²,
 S. Playfer⁵¹, M. Plo Casasus³⁸, T. Poikela³⁹, F. Polci⁸, A. Poluektov^{49,35}, I. Polyakov³²,
 E. Polycarpo², A. Popov³⁶, D. Popov^{11,39}, B. Popovici³⁰, C. Potterat², E. Price⁴⁷, J.D. Price⁵³,
 J. Prisciandaro³⁸, A. Pritchard⁵³, C. Prouve⁴⁷, V. Pugatch⁴⁵, A. Puig Navarro⁴⁰, G. Punzi^{24,s},
 W. Qian⁵⁶, R. Quagliani^{7,47}, B. Rachwal²⁷, J.H. Rademacker⁴⁷, M. Rama²⁴, M. Ramos Pernas³⁸,
 M.S. Rangel², I. Raniuk⁴⁴, G. Raven⁴³, F. Redi⁵⁴, S. Reichert⁵⁵, A.C. dos Reis¹, V. Renaudin⁷,
 S. Ricciardi⁵⁰, S. Richards⁴⁷, M. Rihl³⁹, K. Rinnert^{53,39}, V. Rives Molina³⁷, P. Robbe^{7,39},
 A.B. Rodrigues¹, E. Rodrigues⁵⁵, J.A. Rodriguez Lopez⁶³, P. Rodriguez Perez⁵⁵,

A. Rogozhnikov⁶⁶, S. Roiser³⁹, V. Romanovsky³⁶, A. Romero Vidal³⁸, J. W. Ronayne¹³, M. Rotondo²³, T. Ruf³⁹, P. Ruiz Valls⁶⁷, J.J. Saborido Silva³⁸, N. Sagidova³¹, B. Saitta^{16,f}, V. Salustino Guimaraes², C. Sanchez Mayordomo⁶⁷, B. Sanmartin Sedes³⁸, R. Santacesaria²⁶, C. Santamarina Rios³⁸, M. Santimaria¹⁹, E. Santovetti^{25,l}, A. Sarti^{19,m}, C. Satriano^{26,n}, A. Satta²⁵, D.M. Saunders⁴⁷, D. Savrina^{32,33}, S. Schael⁹, M. Schiller³⁹, H. Schindler³⁹, M. Schlupp¹⁰, M. Schmelling¹¹, T. Schmelzer¹⁰, B. Schmidt³⁹, O. Schneider⁴⁰, A. Schopper³⁹, M. Schubiger⁴⁰, M.-H. Schune⁷, R. Schwemmer³⁹, B. Sciascia¹⁹, A. Sciubba^{26,m}, A. Semennikov³², A. Sergi⁴⁶, N. Serra⁴¹, J. Serrano⁶, L. Sestini²³, P. Seyfert²¹, M. Shapkin³⁶, I. Shapoval^{17,44,g}, Y. Shcheglov³¹, T. Shears⁵³, L. Shekhtman³⁵, V. Shevchenko⁶⁵, A. Shires¹⁰, B.G. Siddi¹⁷, R. Silva Coutinho⁴¹, L. Silva de Oliveira², G. Simi^{23,s}, M. Sirendi⁴⁸, N. Skidmore⁴⁷, T. Skwarnicki⁶⁰, E. Smith⁵⁴, I.T. Smith⁵¹, J. Smith⁴⁸, M. Smith⁵⁵, H. Snoek⁴², M.D. Sokoloff^{58,39}, F.J.P. Soler⁵², F. Soomro⁴⁰, D. Souza⁴⁷, B. Souza De Paula², B. Spaan¹⁰, P. Spradlin⁵², S. Sridharan³⁹, F. Stagni³⁹, M. Stahl¹², S. Stahl³⁹, S. Stefkova⁵⁴, O. Steinkamp⁴¹, O. Stenyakin³⁶, S. Stevenson⁵⁶, S. Stoica³⁰, S. Stone⁶⁰, B. Storaci⁴¹, S. Stracka^{24,t}, M. Straticiu³⁰, U. Straumann⁴¹, L. Sun⁵⁸, W. Sutcliffe⁵⁴, K. Swientek²⁸, S. Swientek¹⁰, V. Syropoulos⁴³, M. Szczekowski²⁹, T. Szumlak²⁸, S. T'Jampens⁴, A. Tayduganov⁶, T. Tekampe¹⁰, G. Tellarini^{17,g}, F. Teubert³⁹, C. Thomas⁵⁶, E. Thomas³⁹, J. van Tilburg⁴², V. Tisserand⁴, M. Tobin⁴⁰, J. Todd⁵⁸, S. Tolk⁴³, L. Tomassetti^{17,g}, D. Tonelli³⁹, S. Topp-Joergensen⁵⁶, E. Tournefier⁴, S. Tourneur⁴⁰, K. Trabelsi⁴⁰, M. Traill⁵², M.T. Tran⁴⁰, M. Tresch⁴¹, A. Trisovic³⁹, A. Tsaregorodtsev⁶, P. Tsopelas⁴², N. Tuning^{42,39}, A. Ukleja²⁹, A. Ustyuzhanin^{66,65}, U. Uwer¹², C. Vacca^{16,39,f}, V. Vagnoni¹⁵, G. Valenti¹⁵, A. Vallier⁷, R. Vazquez Gomez¹⁹, P. Vazquez Regueiro³⁸, C. Vázquez Sierra³⁸, S. Vecchi¹⁷, M. van Veghel⁴³, J.J. Velthuis⁴⁷, M. Veltri^{18,h}, G. Veneziano⁴⁰, M. Vesterinen¹², B. Viaud⁷, D. Vieira², M. Vieites Diaz³⁸, X. Vilasis-Cardona^{37,p}, V. Volkov³³, A. Vollhardt⁴¹, D. Voong⁴⁷, A. Vorobyev³¹, V. Vorobyev³⁵, C. Voß⁶⁴, J.A. de Vries⁴², R. Waldi⁶⁴, C. Wallace⁴⁹, R. Wallace¹³, J. Walsh²⁴, J. Wang⁶⁰, D.R. Ward⁴⁸, N.K. Watson⁴⁶, D. Websdale⁵⁴, A. Weiden⁴¹, M. Whitehead³⁹, J. Wicht⁴⁹, G. Wilkinson^{56,39}, M. Wilkinson⁶⁰, M. Williams³⁹, M.P. Williams⁴⁶, M. Williams⁵⁷, T. Williams⁴⁶, F.F. Wilson⁵⁰, J. Wimberley⁵⁹, J. Wishahi¹⁰, W. Wislicki²⁹, M. Witek²⁷, G. Wormser⁷, S.A. Wotton⁴⁸, K. Wraight⁵², S. Wright⁴⁸, K. Wyllie³⁹, Y. Xie⁶², Z. Xu⁴⁰, Z. Yang³, H. Yin⁶², J. Yu⁶², X. Yuan³⁵, O. Yushchenko³⁶, M. Zangoli¹⁵, M. Zavertyaev^{11,c}, L. Zhang³, Y. Zhang³, A. Zhelezov¹², A. Zhokhov³², L. Zhong³, V. Zhukov⁹, S. Zucchelli¹⁵.

¹Centro Brasileiro de Pesquisas Físicas (CBPF), Rio de Janeiro, Brazil

²Universidade Federal do Rio de Janeiro (UFRJ), Rio de Janeiro, Brazil

³Center for High Energy Physics, Tsinghua University, Beijing, China

⁴LAPP, Université Savoie Mont-Blanc, CNRS/IN2P3, Annecy-Le-Vieux, France

⁵Clermont Université, Université Blaise Pascal, CNRS/IN2P3, LPC, Clermont-Ferrand, France

⁶CPPM, Aix-Marseille Université, CNRS/IN2P3, Marseille, France

⁷LAL, Université Paris-Sud, CNRS/IN2P3, Orsay, France

⁸LPNHE, Université Pierre et Marie Curie, Université Paris Diderot, CNRS/IN2P3, Paris, France

⁹I. Physikalisches Institut, RWTH Aachen University, Aachen, Germany

¹⁰Fakultät Physik, Technische Universität Dortmund, Dortmund, Germany

¹¹Max-Planck-Institut für Kernphysik (MPIK), Heidelberg, Germany

¹²Physikalisches Institut, Ruprecht-Karls-Universität Heidelberg, Heidelberg, Germany

¹³School of Physics, University College Dublin, Dublin, Ireland

¹⁴Sezione INFN di Bari, Bari, Italy

¹⁵Sezione INFN di Bologna, Bologna, Italy

- ¹⁶ *Sezione INFN di Cagliari, Cagliari, Italy*
- ¹⁷ *Sezione INFN di Ferrara, Ferrara, Italy*
- ¹⁸ *Sezione INFN di Firenze, Firenze, Italy*
- ¹⁹ *Laboratori Nazionali dell'INFN di Frascati, Frascati, Italy*
- ²⁰ *Sezione INFN di Genova, Genova, Italy*
- ²¹ *Sezione INFN di Milano Bicocca, Milano, Italy*
- ²² *Sezione INFN di Milano, Milano, Italy*
- ²³ *Sezione INFN di Padova, Padova, Italy*
- ²⁴ *Sezione INFN di Pisa, Pisa, Italy*
- ²⁵ *Sezione INFN di Roma Tor Vergata, Roma, Italy*
- ²⁶ *Sezione INFN di Roma La Sapienza, Roma, Italy*
- ²⁷ *Henryk Niewodniczanski Institute of Nuclear Physics Polish Academy of Sciences, Kraków, Poland*
- ²⁸ *AGH - University of Science and Technology, Faculty of Physics and Applied Computer Science, Kraków, Poland*
- ²⁹ *National Center for Nuclear Research (NCBJ), Warsaw, Poland*
- ³⁰ *Horia Hulubei National Institute of Physics and Nuclear Engineering, Bucharest-Magurele, Romania*
- ³¹ *Petersburg Nuclear Physics Institute (PNPI), Gatchina, Russia*
- ³² *Institute of Theoretical and Experimental Physics (ITEP), Moscow, Russia*
- ³³ *Institute of Nuclear Physics, Moscow State University (SINP MSU), Moscow, Russia*
- ³⁴ *Institute for Nuclear Research of the Russian Academy of Sciences (INR RAN), Moscow, Russia*
- ³⁵ *Budker Institute of Nuclear Physics (SB RAS) and Novosibirsk State University, Novosibirsk, Russia*
- ³⁶ *Institute for High Energy Physics (IHEP), Protvino, Russia*
- ³⁷ *Universitat de Barcelona, Barcelona, Spain*
- ³⁸ *Universidad de Santiago de Compostela, Santiago de Compostela, Spain*
- ³⁹ *European Organization for Nuclear Research (CERN), Geneva, Switzerland*
- ⁴⁰ *Ecole Polytechnique Fédérale de Lausanne (EPFL), Lausanne, Switzerland*
- ⁴¹ *Physik-Institut, Universität Zürich, Zürich, Switzerland*
- ⁴² *Nikhef National Institute for Subatomic Physics, Amsterdam, The Netherlands*
- ⁴³ *Nikhef National Institute for Subatomic Physics and VU University Amsterdam, Amsterdam, The Netherlands*
- ⁴⁴ *NSC Kharkiv Institute of Physics and Technology (NSC KIPT), Kharkiv, Ukraine*
- ⁴⁵ *Institute for Nuclear Research of the National Academy of Sciences (KINR), Kyiv, Ukraine*
- ⁴⁶ *University of Birmingham, Birmingham, United Kingdom*
- ⁴⁷ *H.H. Wills Physics Laboratory, University of Bristol, Bristol, United Kingdom*
- ⁴⁸ *Cavendish Laboratory, University of Cambridge, Cambridge, United Kingdom*
- ⁴⁹ *Department of Physics, University of Warwick, Coventry, United Kingdom*
- ⁵⁰ *STFC Rutherford Appleton Laboratory, Didcot, United Kingdom*
- ⁵¹ *School of Physics and Astronomy, University of Edinburgh, Edinburgh, United Kingdom*
- ⁵² *School of Physics and Astronomy, University of Glasgow, Glasgow, United Kingdom*
- ⁵³ *Oliver Lodge Laboratory, University of Liverpool, Liverpool, United Kingdom*
- ⁵⁴ *Imperial College London, London, United Kingdom*
- ⁵⁵ *School of Physics and Astronomy, University of Manchester, Manchester, United Kingdom*
- ⁵⁶ *Department of Physics, University of Oxford, Oxford, United Kingdom*
- ⁵⁷ *Massachusetts Institute of Technology, Cambridge, MA, United States*
- ⁵⁸ *University of Cincinnati, Cincinnati, OH, United States*
- ⁵⁹ *University of Maryland, College Park, MD, United States*
- ⁶⁰ *Syracuse University, Syracuse, NY, United States*
- ⁶¹ *Pontifícia Universidade Católica do Rio de Janeiro (PUC-Rio), Rio de Janeiro, Brazil, associated to ²*
- ⁶² *Institute of Particle Physics, Central China Normal University, Wuhan, Hubei, China, associated to ³*
- ⁶³ *Departamento de Física, Universidad Nacional de Colombia, Bogota, Colombia, associated to ⁸*
- ⁶⁴ *Institut für Physik, Universität Rostock, Rostock, Germany, associated to ¹²*
- ⁶⁵ *National Research Centre Kurchatov Institute, Moscow, Russia, associated to ³²*

⁶⁶ *Yandex School of Data Analysis, Moscow, Russia, associated to* ³²

⁶⁷ *Instituto de Fisica Corpuscular (IFIC), Universitat de Valencia-CSIC, Valencia, Spain, associated to* ³⁷

⁶⁸ *Van Swinderen Institute, University of Groningen, Groningen, The Netherlands, associated to* ⁴²

^a *Universidade Federal do Triângulo Mineiro (UFMT), Uberaba-MG, Brazil*

^b *Laboratoire Leprince-Ringuet, Palaiseau, France*

^c *P.N. Lebedev Physical Institute, Russian Academy of Science (LPI RAS), Moscow, Russia*

^d *Università di Bari, Bari, Italy*

^e *Università di Bologna, Bologna, Italy*

^f *Università di Cagliari, Cagliari, Italy*

^g *Università di Ferrara, Ferrara, Italy*

^h *Università di Urbino, Urbino, Italy*

ⁱ *Università di Modena e Reggio Emilia, Modena, Italy*

^j *Università di Genova, Genova, Italy*

^k *Università di Milano Bicocca, Milano, Italy*

^l *Università di Roma Tor Vergata, Roma, Italy*

^m *Università di Roma La Sapienza, Roma, Italy*

ⁿ *Università della Basilicata, Potenza, Italy*

^o *AGH - University of Science and Technology, Faculty of Computer Science, Electronics and Telecommunications, Kraków, Poland*

^p *LIFAEELS, La Salle, Universitat Ramon Llull, Barcelona, Spain*

^q *Hanoi University of Science, Hanoi, Viet Nam*

^r *Università di Padova, Padova, Italy*

^s *Università di Pisa, Pisa, Italy*

^t *Scuola Normale Superiore, Pisa, Italy*

^u *Università degli Studi di Milano, Milano, Italy*

[†] *Deceased*